Journal of Materials Chemistry A

ROYAL SOCIETY OF CHEMISTRY

PAPER

View Article Online
View Journal | View Issue

Cite this: *J. Mater. Chem. A*, 2023, **11**, 14933

Catalytic conversion of polyethylene into aromatics with Pt/ZSM-5: insights into reaction pathways and rate-controlling step regulation†

Wenjie Wang,‡[a] Chang Yao,‡[a] Xiaohu Ge,‡[a] Xin Pu,[a] Jiangchun Yuan,[a] Weixiao Sun,[a] Wenyao Chen,[a] Xiang Feng,[b] Gang Qian,[a] Xuezhi Duan,[a] Yueqiang Cao,*[a] Zhirong Yang,*[c] Xinggui Zhou[a] and Jing Zhang*[a]

Catalytic pyrolysis of polyethylene (PE) can produce benzene, toluene, and xylene (BTX) as important building-block chemicals, and selectivity control is key to its economic and ecological efficiency. Here, we report a synergistic effect between Pt and ZSM-5 for selective production of BTX from catalytic pyrolysis of PE by providing mechanistic insights into reaction pathways of key intermediates and regulation of the rate-controlling step. A high yield (52%) of BTX was obtained at 450 °C under atmospheric pressure using a Pt/ZSM-5 catalyst, where Pt mainly exists in the metallic state with a cuboctahedral crystal structure. In contrast, thermal pyrolysis of PE produced linear alkenes/alkanes of wide carbon number distribution, and catalytic pyrolysis of PE over ZSM-5 led to a low BTX yield of 21% with C_1–C_4 alkenes/alkanes being the major products even at a higher temperature (500 °C). It was found that the introduction of Pt into ZSM-5 significantly decreased the aromatization onset temperature, suggesting a reduction of apparent activation energy for the aromatization of alkene intermediates during catalytic pyrolysis of PE. Density functional theory calculations reveal that the aromatization of intermediate ethylene proceeds *via* oligomerization, cyclization, and dehydrogenation, and the energy barrier of the rate-controlling step, *i.e.*, dehydrogenation of $C_6H_{11}^*$, on Pt/ZSM-5 is much lower than that on ZSM-5. As a result, Pt enhanced the aromatization rates of light alkenes formed by PE cracking over the acid sites in ZSM-5, the synergistic effects of which contributed to the high BTX yield on Pt/ZSM-5.

Received 31st March 2023
Accepted 7th June 2023

DOI: 10.1039/d3ta01917a

rsc.li/materials-a

[a]*State Key Laboratory of Chemical Engineering, East China University of Science and Technology, 130 Meilong Road, Shanghai 200237, China. E-mail: yqcao@ecust.edu.cn; jingzhang8507@ecust.edu.cn*

[b]*State Key Lab of Heavy Oil Processing, China University of Petroleum, Qingdao 266580, China*

[c]*School of Chemical Engineering, Zhengzhou University, Zhengzhou 450001, China. E-mail: zhryang@zzu.edu.cn*

† Electronic supplementary information (ESI) available. See DOI: https://doi.org/10.1039/d3ta01917a

‡ These authors contributed equally to this work.

Jing Zhang received his PhD degree in Chemical Engineering from Iowa State University (2014). After being a post-doctoral fellow for four years at the University of Colorado Boulder, he joined the faculty of the Department of Chemical Engineering at East China University of Science and Technology (ECUST) in 2019. He is a full professor and deputy director of the United Laboratory of Chemical Reaction Engineering at ECUST. His current research focuses on conversion of plastics and biomass into fuels and chemicals. He has received the American Institute of Chemists Postdoctoral Award, Outstanding Contribution Award from "Green Chemical Engineering", Youth Research Group Award of Shanghai, etc.

1 Introduction

Global plastic production was 390.7 million tonnes in 2021, 90% of which was derived from fossil resources.[1] The abundant use of plastics has led to a concern for finite natural resources. About half of the annually produced plastic is disposed worldwide each year with landfills and incineration being the major disposal methods, which cause a severe global environmental crisis.[2–5] Approximately 13% of all plastic ever produced has been reused or recycled, and only 1% has undergone high-value chemical recycling.[6,7] Polyethylene (PE) is the largest contributor among plastics, making up ~36% of global plastic production.[8] Notably, the PE waste generated each year accounts for ~85% of annually produced PE.[9] Nowadays, the accumulation rates of waste PE are far beyond the industrial processing capacity. Therefore, development of an efficient recycling method to tackle the rapidly accumulated PE is essential both economically and environmentally.

At present, there are ~20 commercialized plants for catalytic processing of waste PE globally, where 70% of the identified processes are based on catalytic pyrolysis.[10,11] Difficulty in control of product distribution and costly subsequent separation processes severely hindered its commercialization, and the proliferation of companies requires subsidizing policies for plastic waste valorization. The targeted products of these commercial plants can be divided into two categories: (1) benzene, toluene, and xylene (BTX) as basic building block chemicals; (2) oils that include naphtha, gasoline, diesel, *etc.*[12,13] The current work focuses on the catalytic pyrolysis of PE into aromatic products.

Thermal pyrolysis of PE proceeds *via* a radical chain transfer mechanism to generate a broad range of hydrocarbons.[14,15] To narrow the product distribution and lower the reaction temperature, catalytic pyrolysis has been used mainly with zeolites, such as ZSM-5, ZSM-11, Hβ, HY, USY, REY, FCC, *etc.*, where catalytic cracking mainly proceeds through carbocation intermediates.[16–21] It was proposed that PE is first cracked by the Brønsted acid sites on the external surface of zeolites, and then, the resulting intermediates may enter the zeolite micropore for further reactions over its confined strong Brønsted acid sites to generate light alkenes/alkanes and aromatics.[22] A significant amount of BTX production from catalytic pyrolysis often requires 500 °C or higher temperatures.[23–25] Among the zeolite catalysts, ZSM-5 was reported to facilitate BTX formation from hydrocarbon intermediates, due to the unique shape selectivity and hindrance of coke growth derived from its pore structure.[26,27] Low BTX yields (~20%) were obtained from catalytic pyrolysis of PE regardless of ZSM-5.[20] Although Zn and Ga modified zeolites have been reported to promote BTX production from PE, the role of metal and its synergy with zeolites were not studied.[28–30] Furthermore, there is a lack of mechanistic insights into reaction pathways of key intermediates for catalytic conversion of PE into aromatics over zeolite catalysts. Aromatization of light alkenes over zeolites was proposed to proceed *via* condensation, cyclization, and dehydrogenation reactions, among which dehydrogenation was regarded as the slow step.[20,31,32] Therefore, BTX production from catalytic pyrolysis of PE over zeolites may be hindered by the slow dehydrogenation rates of aromatic precursors. In this regard, incorporating metals that are capable of dehydrogenation (for example, Pt) into ZSM-5 may be desirable to promote dehydrogenation and thus enhance the BTX yield from PE.

Here, we report a synergistic effect between Pt and ZSM-5 for selective production of BTX from catalytic pyrolysis of PE by providing mechanistic insights into reaction pathways of key intermediates and structures of rate-controlling transition states. Catalyst characterization reveals that Pt mainly exists in the metallic state with a cuboctahedral crystal structure and loading Pt onto ZSM-5 did not apparently change the nature of acid sites in zeolites. Thermal pyrolysis of PE produced linear alkenes/alkanes with a wide distribution of carbon number. Catalytic pyrolysis of PE over ZSM-5 at the same temperature (500 °C) mainly generated C_1–C_4 alkenes/alkanes (65.5%, total yield) and BTX (21.1%, total yield), while the BTX yield markedly increased to 52.4% even at a lower temperature (450 °C) at the expense of light alkenes after introduction of Pt into ZSM-5. The onset temperature of aromatization also decreased for Pt/ZSM-5, suggesting a reduction in apparent activation energy for the aromatization of light alkene intermediates. Density function theory (DFT) calculations reveal that the aromatization of ethylene, a key intermediate in catalytic pyrolysis of PE over ZSM-5 and Pt/ZSM-5, proceeds *via* oligomerization, cyclization, and dehydrogenation, where a much lower energy barrier for the proposed rate-controlling step (dehydrogenation) was obtained for Pt/ZSM-5 compared to ZSM-5. This difference is presumably due to the different nature of sites for the β-hydrogen abstraction in Pt/ZSM-5 and ZSM-5. As a result, Pt enhanced the aromatization rates of light alkenes formed by PE cracking over the acid sites in ZSM-5, the collective effects of which contributed to the high BTX yield. The insights reported here may pave the way for the design of "metal–zeolite" catalysts for efficient conversion of polyolefins into BTX.

2 Methods

2.1 Catalyst preparation

The PE in this work was purchased from Sigma-Aldrich in a powder form. ZSM-5 catalysts with different SiO_2/Al_2O_3 ratios were purchased from Jiangsu Xianfeng Nanomaterial Technology Co., Ltd. All the supported metal catalysts were prepared by the incipient wetness impregnation of metal on the ZSM-5 (38) support. After impregnation, the samples were aged at room temperature for 2 hours, and then dried at 120 °C overnight. Finally, the samples were calcined at 550 °C in air for 3 hours.

2.2 Catalyst characterization

Metal loadings on the catalysts were determined in the catalyst by using an inductively coupled plasma-optical emission spectrometer (ICP-OES, Agilent 725). Textural properties of the catalysts, including specific surface area, pore volume, and pore size distribution, were measured *via* N_2 adsorption–desorption

using a Micromeritics Tristar 3Flex with the Brunauer–Emmet–Teller (BET), *t*-plot and Barrett–Joyner–Halenda (BJH) methods. The crystallographic structures of metal/ZSM-5 catalysts were analyzed by X-ray diffraction (XRD) using a Bruker D8 XRD. Scanning electron microscopy (SEM, FEI Nova NanoSEM 450) and high-angle annular dark-field scanning transmission electron microscopy (HADDF-STEM, Thermo Fisher Talos F200X), with energy dispersive spectroscopy (EDS), were used to determine the morphology of ZSM-5 (38) and the size of Pt on Pt/ZSM-5 (38). Aberration-corrected STEM (AC-STEM) analysis and fast Fourier transform (FFT) analysis were performed with a Thermo Fisher Themis Z microscope to obtain lattice information of ZSM-5 and Pt. The acid properties of the catalysts were evaluated *via* NH_3 temperature-programmed desorption (NH_3-TPD, Micromeritics Auto Chem II 2920) and pyridine adsorption FT-IR (Py-IR, Bruker ALPHA, Germany). X-ray photoelectron spectroscopy (XPS) analysis was performed with a Thermo Fisher Nexsa spectrometer to characterize the states of Pt species on ZSM-5. The metal dispersion on ZSM-5 was determined by CO-chemisorption using a Micromeritics Auto Chem II 2920. Thermogravimetric analysis (TGA) was performed using a PerkinElmer Pyris1 thermal gravimetric analyzer. Details of the characterization are given in the ESI Methods.†

2.3 Catalytic reactions

A scheme of the micropyrolyzer (Frontier Laboratories, Japan) used for the current thermal/catalytic pyrolysis is shown in Fig. S1.† For a typical catalytic reaction, physical mixtures of PE and the catalyst were loaded into a deactivated stainless cup and then dropped into a preheated furnace. The products of the catalytic pyrolysis were analyzed online by GC/MS-FID-TCD (Agilent 7890B/5977B). He was used as the carrier gas with a flow rate of 55 mL min^{-1}. The products were split into two streams after entering the GC. One stream flowed through a capillary column (GC-GasPro, 60 m × 320 μm × 0 μm, Agilent, USA) to reach a thermal conductivity detector (TCD), and the other stream flowed through a capillary column (HP-5, 30 m × 320 μm × 0.25 μm, Agilent, USA) to reach a mass spectrometer (MS 5977B, Agilent, USA) or a flame ionization detector (FID).

2.4 DFT calculations

All density functional theory (DFT) calculations were performed using the Vienna *Ab initio* Simulation Package (VASP) with the Perdew–Burke–Ernzerhof (PBE) functional and projected-augmented wave (PAW). The generalized gradient approximation (GGA) was utilized to accurately describe the exchange–correlation functionals.[33] Furthermore, empirical dispersion correction (DFT-D3) was included in all calculations to account for van der Waals interactions.[34] ZSM-5 zeolite is a widely used catalyst in the petrochemical industry due to its MFI framework topology and three-dimensional pore structure. According to the literature, two Si atoms at T8 and T12 sites can be replaced by two Al atoms to establish a ZSM-5 zeolite model.[31] A Pt13 cluster was placed on the optimized ZSM-5 surface to construct a Pt/ZSM-5 model. The dimer method was utilized to locate the transition states of elementary steps.

The adsorption energy (E_{ads}) of the adsorbed species on the catalyst was calculated using the equation:

$$E_{ads} = E_{total} - E_{surface} - E_{absorbate}$$

where E_{total}, $E_{surface}$ and $E_{absorbate}$ represent the total energy of the surface and absorbate, the energy of the clean surface, and the energy of the isolated absorbate, respectively.

The reaction activation energy (E_a) was calculated by using the equation:

$$E_a = E_{TS} - E_{IS}$$

where E_{TS} and E_{IS} are the total energies of the transition state (TS) and initial state (IS), respectively.

3 Results and discussion

3.1 Characteristics of the material

Chemical and physical properties of the currently used polyethylene (PE) are shown in Table S1.† Its number average (M_n) and weight average (M_w) molecular weight is ~1700 Da and ~4000 Da, respectively, with a density of 0.92 g mL^{-1} at 25 °C, suggesting it is low density polyethylene (LDPE). The elemental analysis of PE shows a very low content of impurities. The obtained contents of C and H are 85.04 wt% and 14.84 wt%, respectively, which are close to the theoretical values of PE (Table S1†). Meanwhile, the thermogravimetric analysis shows that the moisture content of PE is also very low (Fig. S2†).

3.2 Characteristics of catalysts

The textural properties of Pt/ZSM-5 (38) and ZSM-5 catalysts with different SiO_2/Al_2O_3 ratios are shown in Tables 1 and S2,† among which ZSM-5 (38) has the largest specific surface area that is mainly contributed by micropores. The specific surface area was reduced after loading Pt, whereas the pore size was minimally affected. Fig. 1a shows that the N_2 adsorption–desorption isotherms of these catalysts are type I, which corresponds to the micropore filling phenomenon of the zeolites.[35] The pore size distribution obtained by the BJH method shows that these catalysts mainly consist of micropores that are less than 1 nm (Fig. 1b). There are also a few mesopores, the size of which is mainly in the range of 2–3 nm for ZSM-5 (38), ZSM-5 (70), and Pt/ZSM-5 (38) and 3–4 nm for ZSM-5 (25).

The XRD patterns of these ZSM-5 catalysts show five diffraction peaks that correspond to the (1 0 1), (2 0 0), (3 3 2), (3 0 3) and (1 3 3) planes of ZSM-5 material according to their standard JCPDS 44-0003 card, the first two of which are in the range of 7°–10° and the latter three are in the range of 22°–25° (Fig. 1c).[36] Fig. 1d and S3† show that the addition of metals (Pt, Pd, Ru, and Ni) had no apparent effect on the zeolite structure as the MFI structure was retained after loading these metals. The diffraction peaks of Pt (111) and Pt (100) appear for Pt/ZSM-5 (38), suggesting the formation of Pt nanoparticles.[37] In contrast, the XRD patterns of ZSM-5 (38) loaded with Pd, Ni and

Table 1 Physicochemical properties of the catalysts

Catalysts	SiO_2/Al_2O_3	Pt[a] (wt%)	S_{BET}[b] ($m^2\ g^{-1}$)	Pore volume[b] ($cm^3\ g^{-1}$)	Pore size[b] (nm)
ZSM-5 (25)	25	—	263.9	0.192	3.67
ZSM-5 (38)	38	—	345.7	0.182	2.23
ZSM-5 (70)	70	—	239.5	0.142	2.97
Pt/ZSM-5 (38)	38	1.4	309.8	0.164	2.26

[a] Elemental compositions of the catalysts were determined by ICP-AES. [b] Textural structure was obtained by N_2 physical adsorption–desorption.

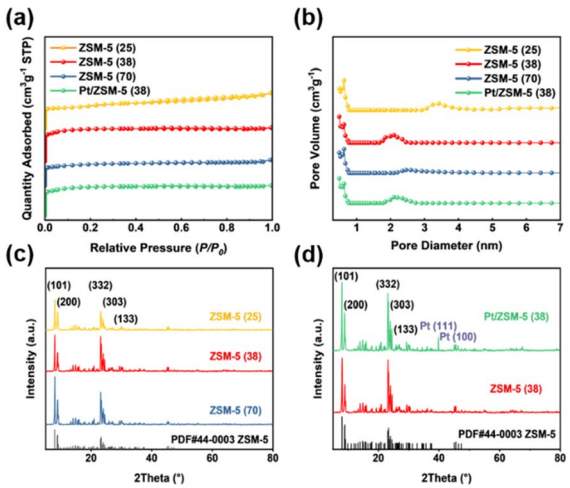

Fig. 1 (a) N_2 adsorption–desorption isotherms and (b) BJH distribution of Pt/ZSM-5 (38) and ZSM-5 (38) catalysts with different SiO_2/Al_2O_3 ratios. (c) XRD patterns of ZSM-5 catalysts with different SiO_2/Al_2O_3 ratios. (d) XRD patterns of ZSM-5 (38) and Pt/ZSM-5 (38).

Ru did not show diffraction peaks of these metals and their oxides, indicating that these metals are highly dispersed on zeolites (Fig. S3†).[38]

NH_3-TPD analysis of these catalysts shows wide NH_3 desorption peaks in the range of 100–600 °C, where the signals below and above 350 °C can be assigned to NH_3 desorption from weak and moderate–strong acid sites, respectively.[39,40] The acid strength increased with the increasing SiO_2/Al_2O_3 ratio of ZSM-5, as suggested by the peaks of moderate–strong acid sites shifting to higher temperatures (Fig. S4†).

The .acid strength remains unchanged after loading Pt on ZSM-5 (38). To further study the nature of acid sites and their strength, pyridine-IR (Py-IR) spectra were collected at elevated temperatures (50 °C, 150 °C, 200 °C, and 350 °C). The bands at 1450 cm^{-1} and 1550 cm^{-1} represent the interaction of pyridine with Lewis acid and Brønsted acid sites, respectively, while the peaks at 1490 cm^{-1} are attributed to the sum of Lewis acid and Brønsted acid sites.[41] According to the semi-quantitative analysis in Fig. 2a, S5 and Table S3,† signals of both Brønsted acid and Lewis acid sites decreased with increasing temperature, and the one for Lewis acid decreased more rapidly. Therefore, the NH_3 desorption in the range of 100–300 °C was mainly derived from weakly bonded NH_3 on Lewis acid sites of ZSM-5 catalysts. The relatively stronger Brønsted acid sites may be derived from the Si–O(H)–Al structure.[42] The Py-IR analysis also suggests that the introduction of Pt did not apparently change the nature of acid sites and their strength (Fig. 2b).

As can be seen from the SEM images, ZSM-5 (38) is mainly in the form of lath-shaped hexagonal crystals, which is a typical shape of the MFI structure (Fig. 3a).[43] It was reported that the SiO_2/Al_2O_3 ratio of typical hexagonal clusters is 36, which is similar to the one of ZSM-5 (38) used in this work. HADDF-STEM analysis shows that the average Pt particle size of Pt/ZSM-5 (38) is 2.30 nm with a wide distribution (Fig. 3b). Therefore, the Pt particles/clusters may exist both on the external surface and in micropores of ZSM-5. The pore structure of the ZSM-5 catalyst can be observed by AC-HAADF-STEM (Fig. 3c), which shows a micropore size of ~0.55 nm. The Pt nanoparticles shown in Fig. S6† exhibit lattice spacings of 2.23

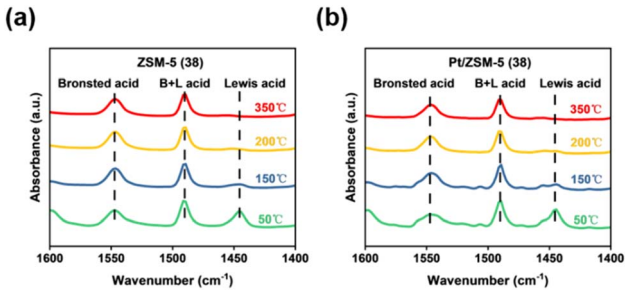

Fig. 2 (a) Pyridine-IR spectra of the ZSM-5 (38) catalyst. (b) Pyridine-IR spectra of the Pt/ZSM-5 (38) catalyst.

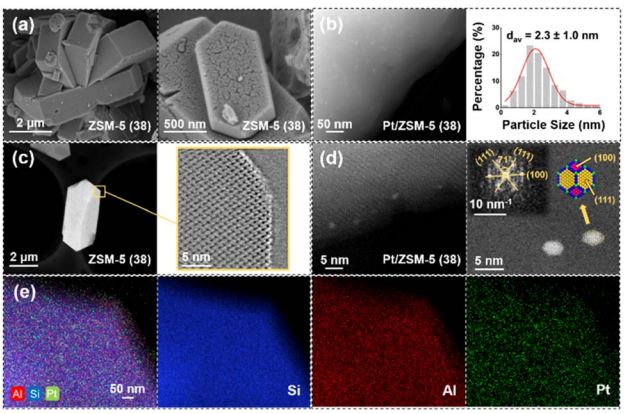

Fig. 3 (a) SEM images of ZSM-5 (38). (b) HADDF-STEM images and particle size distribution of Pt/ZSM-5 (38). (c) AC-HAADF-STEM images of ZSM-5 (38). (d) AC-HAADF-STEM images of Pt/ZSM-5 (38). (e) HAADF-STEM images and elemental mappings of Pt/ZSM-5 (38).

Å and 1.97 Å, corresponding to the (111) and (100) planes of Pt on ZSM-5, respectively.[44,45] The fast Fourier transform (FFT) model of the atomic image shows that the Pt nanoparticles exist in the form of a cuboctahedron (Fig. 3d).[46] EDS scanning results show that Pt was uniformly dispersed on ZSM-5 (38) (Fig. 3e).

XPS analysis shows that the spectrum of Pt on ZSM-5 consists of two peaks at $4d_{3/2}$ and $4d_{5/2}$,[47] the deconvolution of which leads to two peaks centered at 314.6 eV and 332.0 eV (Pt^0 species) and another two peaks centered at 317.3 eV and 335.2 eV (Pt^{2+} species).[48] The areas of the deconvoluted peaks indicate that Pt on ZSM-5 mainly exists in the metallic state (Fig. S7†).

In summary, the characterization results showed that (1) loading Pt on ZSM-5 did not apparently change the nature and strength of acid sites on the zeolite where Brønsted acid sites are stronger than Lewis acid sites; (2) the Pt nanoparticles mainly exist in the metallic state with a cuboctahedral shape.

3.3 Catalytic reactions and results

Thermal pyrolysis of PE at 500 °C resulted in a wide distribution of hydrocarbon products ranging from C_1 to C_{54} (Fig. 4a, S8 and Table S4†). In general, at each carbon number the liquid products (C_{5+}) consist of the corresponding alkane, olefin and diolefin, where the olefin is the major component with a total yield of 51.8%. On the other hand, the gas products consist of alkanes and alkenes. For catalytic pyrolysis of PE over ZSM-5 (38), the product distribution became markedly narrower (C_1 to C_{13}), where monoaromatics are the major liquid products and the gas products mainly consist of alkanes and alkenes (Fig. 4a and Table S5†). Compared to thermal pyrolysis, catalytic pyrolysis over ZSM-5 (38) facilitated the formation of BTX (20.3%, total yield) and gas products (60.7%, total yield) (Tables S4, S5 and Fig. S9†). It was proposed that the external Brønsted acid sites of ZSM-5 promote the PE cracking into smaller hydrocarbons. These intermediates then enter ZSM-5 micropores where the collective effects of shape selectivity and relatively stronger Brønsted acid sites facilitate secondary cracking, oligomerization, cyclization and dehydroaromatization to form light alkanes/alkenes and aromatics.[22]

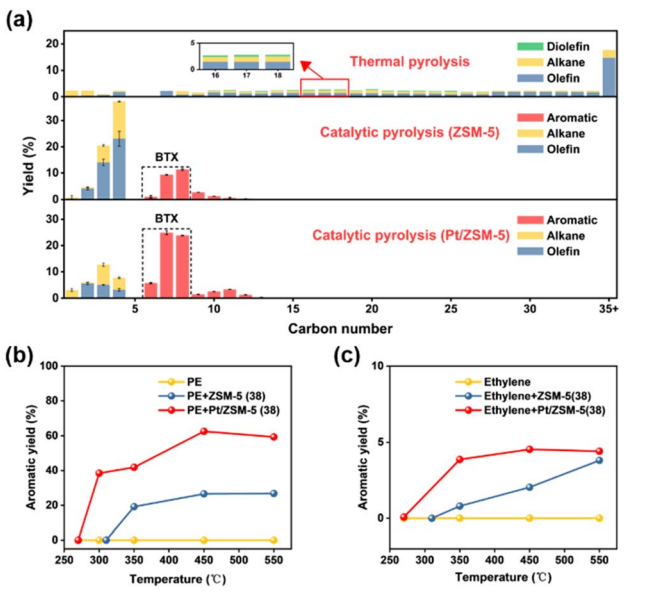

Fig. 4 (a) Product distribution from thermal pyrolysis (500 °C) and catalytic pyrolysis (450 °C) of PE. (b) Total yield of aromatics from thermal/catalytic pyrolysis of PE at different temperatures. (c) Total yield of aromatics from catalytic conversion of ethylene at different temperatures.

First, the effect of catalyst loading and reaction temperature on catalytic pyrolysis of PE over ZSM-5 was investigated. Fig. S10 and Table S6† show that the total yield of gas and liquid products increased with increasing catalyst loading and reached a maximal value of 98.6% at a PE to ZSM-5 ratio of 1 : 6, suggesting that a sufficient contact time between the catalyst and feedstock (or intermediates) is beneficial for the formation of aromatics and gas products. Further increasing the catalyst loading slightly lowered the liquid/gas product yield and resulted in more coke, possibly due to enhanced oligomerization/polymerization and/or hydride transfer reactions.[49] Fig. S11 and Table S7† show that the total yield of liquid products (mainly consisting of monoaromatics) reached a maximal value of 33.1% when increasing the reaction temperature from 350 °C to 500 °C, suggesting that aromatization of PE pyrolysis intermediates over ZSM-5 requires a high temperature. Then, the effect of the SiO_2 to Al_2O_3 ratio of ZSM-5 on the catalytic pyrolysis of PE was investigated. Compared to ZSM-5 (25) and ZSM-5 (70), ZSM-5 (38) showed the highest BTX yield of 21.1% (Fig. S12 and Table S8†), possibly due to its moderate acid strength and number of acid sites.

Although ZSM-5 was reported to be effective in producing BTX during hydrocarbon processing, the major products from catalytic pyrolysis of PE over ZSM-5 are C_2–C_4 alkenes with a total yield of 40.1%, while the BTX yield is only 20.3%. Therefore, the experimental results suggest that under the current conditions the rates of aromatization are not sufficient to convert most C_2–C_4 intermediates into BTX. For the alkene aromatization over ZSM-5, dehydrogenation was proposed to be the slow step and speculated to have a high barrier within the reaction path.[31] Hence, incorporating metals that are capable of dehydrogenation into ZSM-5 may be desirable to promote dehydrogenation and thus enhance the BTX yield from catalytic pyrolysis of PE. Then, Pt/ZSM-5, Pd/ZSM-5, Ni/ZSM-5 and Ru/ZSM-5 catalysts were evaluated for the catalytic pyrolysis of PE, where different degrees of BTX yield increase were observed compared to the one from ZSM-5 (Fig. S13 and Table S9†). Similar metal loadings were used for the above catalysts, from which Pt/ZSM-5 showed the highest BTX yield (52.4%), accounting for 84.1% of the liquid products (Fig. 4a, S14 and Table S12†). Meanwhile, the total yield of light alkenes decreased significantly from 40.1% to 13.7% after loading Pt on ZSM-5 (Table S5†). The difference in catalytic performance among different metals may be derived from the distribution of these metals and/or their influence on the barriers of the rate-limiting step during aromatization. Then, the catalyst loadings and reaction temperature were optimized for the catalytic pyrolysis of PE over Pt/ZSM-5 (Fig. S15, S16, Tables S10, and S11†). Under optimized conditions, we also performed catalytic cracking of a PE film (food grade, MIAOJIE) over the Pt/ZSM-5

catalyst. The results show that the yield of BTX is 53.2%, which is similar as the aforementioned yield (52.4%) from the PE powder (Sigma-Aldrich). The small difference in the yield of liquid, gas, and solid products may be attributed to the presence of additives in these PE (Fig. S17 and Table S12†). A recyclability test for the catalytic pyrolysis of PE over Pt/ZSM-5 was also performed. The results showed that the BTX yield remained at a high level during four consecutive runs, and a slight decrease was observed in the first three runs (Fig. S18 and Table S13†).

We speculated that the addition of Pt on ZSM-5 lowered the apparent activation energy of aromatization during the catalytic pyrolysis of PE. For verification, the catalytic pyrolysis of PE was performed at elevated temperatures over ZSM-5 and Pt/ZSM-5, respectively, the results of which show that the onset temperature for aromatics formation decreased from 310 °C (ZSM-5) to 270 °C (Pt/ZSM-5) (Fig. 4b). Since the addition of Pt significantly increased the BTX yield at the expense of C_2–C_4 alkenes, the latter was regarded as the intermediate for BTX formation during the catalytic pyrolysis of PE. In this regard, ethylene was chosen as the major intermediate and underwent aromatization over ZSM-5 and Pt/ZSM-5 at different temperatures (Fig. 4c). A very similar change of onset temperature for aromatics formation was observed for ethylene, as compared to the one for PE, further suggesting that Pt lowered the apparent activation energy for light alkene aromatization and thereby enhanced the BTX yield during the catalytic pyrolysis of PE.

In summary, the thermal and catalytic pyrolysis of PE showed that (1) thermal pyrolysis resulted in a wide distribution of hydrocarbon products (C_1 to C_{54}) consisting of olefins, alkanes, and diolefins, where the olefins are the major component (51.8%, total yield); (2) catalytic pyrolysis over ZSM-5 promoted the formation of BTX (20.3%, total yield) and C_2–C_4 alkenes (40.1%, total yield) due to cracking, oligomerization, cyclization and dehydroaromatization that were catalyzed by acid sites of ZSM-5; (3) the introduction of Pt into ZSM-5 markedly enhanced the BTX yield (52.4%) at the expense of C_2–C_4 alkenes which were intermediates for aromatization; (4) the lower onset temperature for BTX formation over Pt/ZSM-5 suggested that Pt reduced the apparent activation energy for light alkene aromatization. It should be noted that carbon balances over 90% were achieved in most cases.

3.4 Mechanistic study

To provide mechanistic insights into how Pt affects the aromatization of alkene intermediates over ZSM-5, we theoretically investigated the pathways of ethylene (a key intermediate) oligomerization, cyclization, and dehydrogenation to form benzene. The transition state of the dehydrogenation step and the corresponding energy barrier were studied since dehydrogenation was proposed to be the rate-controlling step during the alkene aromatization over zeolites.[32,50] For both ZSM-5 and Pt/ZSM-5, the adsorbed ethylene molecule undergoes two consecutive oligomerization reactions to form alkyl fragments of "$Si-OH+C_6H_{11}^*$" and "$Pt-H+C_6H_{11}^*$", followed by a cyclization step to generate "$Si-OH+6MR\text{-}C_6H_{11}^*$" and "$Pt-H+6MR\text{-}C_6H_{11}^*$", respectively (Fig. 5). Then, the cyclic intermediates go through dehydrogenation *via* formation of hydrocarbon carbocations, where the β-H abstractions need to overcome barriers of 2.79 eV and 1.39 eV to form "$Si-OH+C_6H_{10}^*+H^*$" and "$Pt-H+C_6H_{10}^*+H^*$", respectively, according to the located structures of the corresponding transition states (Fig. 5 and S19–S23†). Benzene would be formed after further step-by-step dehydrogenation through a similar process.

These theoretical calculations demonstrate a much lower energy barrier for the dehydrogenation of C_6 cyclic intermediates over Pt/ZSM-5, as compared to that over ZSM-5, which is

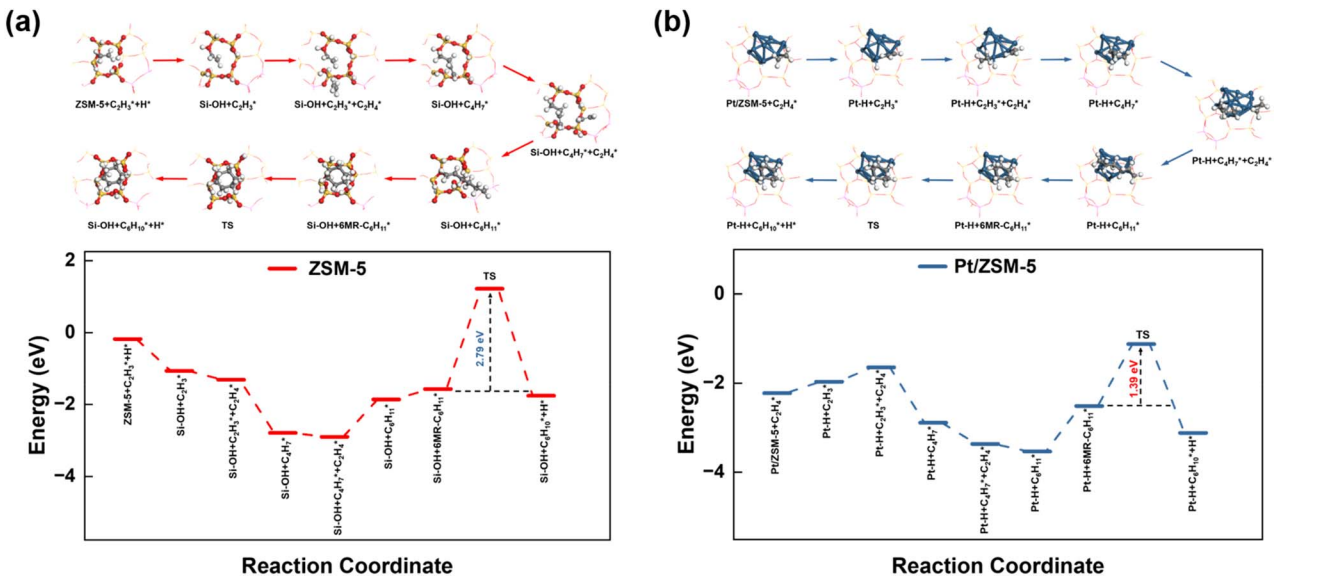

Fig. 5 Reaction energy diagram of ethylene oligomerization, cyclization and dehydrogenation to the benzene precursor over (a) ZSM-5 (38) and (b) Pt/ZSM-5 (38). (Pink: Al, yellow: Si, red: O, grey: C, white: H, and blue: Pt.)

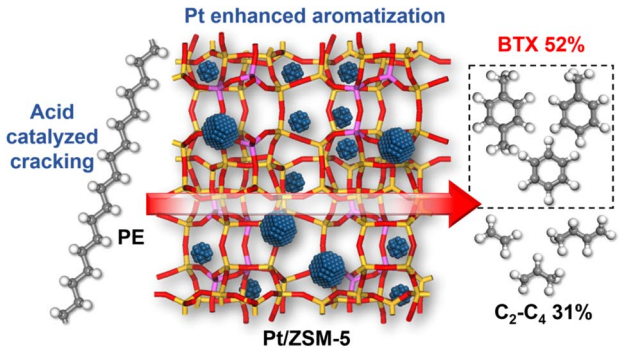

Fig. 6 Proposed scheme showing the synergistic effect in Pt/ZSM-5.

consistent with the markedly improved BTX yield and reduced onset temperature for BTX formation from catalytic pyrolysis of PE over Pt/ZSM-5. The difference may be derived from the different nature of sites for β-hydrogen abstraction in Pt/ZSM-5 and ZSM-5. As a result, Pt enhanced the aromatization rates of light alkenes formed by PE cracking over the acid sites in ZSM-5, leading to the high BTX yield (Fig. 6).

4 Conclusions

In summary, we report a synergistic effect between Pt and ZSM-5 for efficient production of BTX *via* catalytic pyrolysis of PE by providing mechanistic insights into reaction pathways of key intermediate species and regulation of the rate-controlling step. Catalyst characterization reveals that the Pt particles mainly exist in the metallic state with a cuboctahedral shape and their loading on ZSM-5 did not apparently change the nature of acid sites. Different from the thermal pyrolysis of PE that produced linear alkenes/alkanes with a wide carbon number distribution, the catalytic pyrolysis with ZSM-5 at 500 °C mainly generated C_1–C_4 alkenes/alkanes (66%, total yield) and BTX (21%, total yield). The BTX yield markedly increased to 52% at the expense of light alkenes after introduction of Pt to ZSM-5, even at a lower temperature of 450 °C. The onset temperature of aromatization also decreased, suggesting a reduction of apparent activation energy for the aromatization of light alkene intermediates over Pt/ZSM-5. DFT calculations reveal that the aromatization of intermediate ethylene proceeds *via* oligomerization, cyclization and dehydrogenation, and the introduction of Pt into ZSM-5 significantly lowered the energy barrier of the rate-controlling step (dehydrogenation). This difference is presumably due to the different nature of sites for β-hydrogen abstraction in Pt/ZSM-5 against ZSM-5. Therefore, Pt boosted the aromatization rates of light alkenes produced by PE cracking over the acid sites in ZSM-5, resulting in the markedly improved BTX yield. The insights provided here open a new avenue for the design of "metal–zeolite" catalysts for selective conversion of PE into BTX.

Author contributions

WW, CY and XG conducted the experiments, performed density functional theory calculations, collected data and wrote the paper. JZ, ZY, and YC conceived the work, designed the research, supervised the experiment, and edited the paper. JY conducted the AC-HAADF-STEM test under the guidance of WS and WC. XZ, XD, GQ, XP and XF assisted in data analysis and discussion. All authors contributed to the manuscript revision.

Conflicts of interest

There are no conflicts to declare.

Acknowledgements

This work was financially supported by the National Key R&D Program of China (2022YFA1503502 and 2022YFA1503503), the National Natural Science Foundation of China (22008074, 21991103, 22008067, 22008072, and 21991104), Shanghai Rising-star Program (23QA1401900) and the Natural Science Foundation of Shanghai (20ZR1415700).

Notes and references

1 Plastics Europe, *Plastics – The Facts 2022*, **https://plasticseurope.org/knowledge-hub/plastics-the-facts-2022/**.
2 R. Geyer, J. R. Jambeck and K. L. Law, *Sci. Adv.*, 2017, **3**, e1700782.
3 J. M. Garcia and M. L. Robertson, *Science*, 2017, **358**, 870–872.
4 N. M. Wang, G. Strong, V. DaSilva, L. J. Gao, R. Huacuja, I. A. Konstantinov, M. S. Rosen, A. J. Nett, S. Ewart, R. Geyer, S. L. Scott and D. Guironnet, *J. Am. Chem. Soc.*, 2022, **144**, 18526–18531.
5 C. Ostle, R. C. Thompson, D. Broughton, L. Gregory, M. Wootton and D. G. Johns, *Nat. Commun.*, 2019, **10**, 1622.
6 Y. Liu, X. C. Wang, Q. Y. Li, T. R. Yan, X. X. Lou, C. Y. Zhang, M. H. Cao, L. Zhang, T. K. Sham, Q. Zhang, L. He and J. X. Chen, *Adv. Funct. Mater.*, 2023, **33**, 2210283.
7 H. Thomas, M. Mirijam, M. N. Chris, J. S. Theo and W. Christof, *Recycling and the future of the plastics industry*, **https://www.mckinsey.com/industries/chemicals/our-insights/how-plastics-waste-recycling-could-transform-the-chemical-industry**.
8 J. E. Rorrer, C. Troyano-Valls, G. T. Beckham and Y. Roman-Leshkov, *ACS Sustainable Chem. Eng.*, 2021, **9**, 11661–11666.
9 M. Y. Chu, X. P. Wang, X. C. Wang, X. X. Lou, C. Y. Zhang, M. H. Cao, L. Wang, Y. Y. Li, S. B. Liu, T.-K. Sham, Q. Zhang and J. X. Chen, *Research*, 2023, **6**, 0032.
10 A. J. Martin, C. Mondelli, S. D. Jaydev and J. Perez-Ramirez, *Chem*, 2021, **7**, 1487–1533.
11 I. Vollmer, M. J. F. Jenks, M. C. P. Roelands, R. J. White, T. v. Harmelen, P. d. Wild, G. P. v. d. Laan, F. Meirer, J. T. F. Keurentjes and B. M. Weckhuysen, *Angew. Chem., Int. Ed.*, 2020, **59**, 15402–15423.
12 S. L. Lu, Y. X. Jing, B. Feng, Y. Guo, X. H. Liu and Y. Q. Wang, *ChemSusChem*, 2021, **14**, 4242–4250.
13 M. X. Ye, Y. Y. Li, Z. R. Yang, C. Yao, W. X. Sun, X. X. Zhang, W. Y. Chen, G. Qian, X. Z. Duan, Y. C. Cao, L. N. Li,

X. G. Zhou and J. Zhang, *Angew. Chem., Int. Ed.*, 2023, e202301024.
14 L. O. Mark, M. C. Cendejas and I. Hermans, *ChemSusChem*, 2020, **13**, 5808–5836.
15 D. P. Serrano, J. Aguado and J. M. Escola, *ACS Catal.*, 2012, **2**, 1924–1941.
16 S. Kumar, A. K. Panda and R. K. Singh, *Resour. Conserv. Recycl.*, 2011, **55**, 893–910.
17 X. Q. Jia, C. Qin, T. Friedberger, Z. B. Guan and Z. Huang, *Sci. Adv.*, 2016, **2**, e1501591.
18 L. X. Chen, Y. F. Zhu, L. C. Meyer, L. V. Hale, T. T. Le, A. Karkamkar, J. A. Lercher, O. Y. Gutierrez and J. Szanyi, *React. Chem. Eng.*, 2022, **7**, 844–854.
19 Z. W. Dong, W. J. Chen, K. Q. Xu, Y. Liu, J. Wu and F. Zhang, *ACS Catal.*, 2022, **12**, 14882–14901.
20 G. Lopez, M. Artetxe, M. Amutio, J. Bilbao and M. Olazar, *Renewable Sustainable Energy Rev.*, 2017, **73**, 346–368.
21 M. Y. Chu, Y. Liu, X. X. Lou, Q. Zhang and J. X. Chen, *ACS Catal.*, 2022, **12**, 4659–4679.
22 J. D. Duan, W. Chen, C. T. Wang, L. Wang, Z. Q. Liu, X. F. Yi, W. Fang, H. Wang, H. Wei, S. D. Xu, Y. W. Yang, Q. W. Yang, Z. B. Bao, Z. G. Zhang, Q. L. Ren, H. Zhou, X. D. Qin, A. M. Zheng and F. S. Xiao, *J. Am. Chem. Soc.*, 2022, **144**, 14269–14277.
23 P. T. Williams and E. A. Williams, *J. Anal. Appl. Pyrolysis*, 1999, **51**, 107–126.
24 M. L. Mastellone, F. Perugini, M. Ponte and U. Arena, *Polym. Degrad. Stab.*, 2002, **76**, 479–487.
25 M.-H. Cho, S.-H. Jung and J.-S. Kim, *Energy Fuels*, 2010, **24**, 1389–1395.
26 N. Miskolczi, A. Angyal, L. Bartha and I. Valkai, *Fuel Process. Technol.*, 2009, **90**, 1032–1040.
27 A. Chatterjee, D. Bhattacharya, M. Chatterjee and T. Iwasaki, *Microporous Mesoporous Mater.*, 1999, **32**, 189–198.
28 M. S. Renzini, U. Sedran and L. B. Pierella, *J. Anal. Appl. Pyrolysis*, 2009, **86**, 215–220.
29 J. X. Song, J. Wang, Y. H. Pan, X. D. Du, J. Y. Sima, C. X. Zhu, F. F. Lou and Q. X. Huang, *J. Environ. Manage.*, 2022, **322**, 116096.
30 L. C. Fu, Q. A. Xiong, Q. H. Wang, L. Cai, Z. H. Chen and Y. F. Zhou, *ACS Sustainable Chem. Eng.*, 2022, **10**, 9612–9623.
31 H. H. Fan, X. W. Nie, H. Z. Wang, M. J. Janik, C. S. Song and X. W. Guo, *Catal. Sci. Technol.*, 2020, **10**, 8359–8373.
32 C. Y. Tu, H. H. Fan, D. Wang, N. Rui, Y. H. Du, S. D. Senanayake, Z. H. Xie, X. W. Nie and J. G. G. Chen, *Appl. Catal., B*, 2022, **304**, 120956.
33 P. E. Blöchl, *Phys. Rev. B: Condens. Matter Mater. Phys.*, 1994, **50**, 17953–17979.
34 P. A. Korzhavyi, I. A. Abrikosov, B. Johansson, A. V. Ruban and H. L. Skriver, *Phys. Rev. B: Condens. Matter Mater. Phys.*, 1999, **59**, 11693–11703.
35 J. H. Yang, S. X. Yu, H. Y. Hu, Y. Zhang, J. M. Lu, J. Q. Wang and D. H. Yin, *Chem. Eng. J.*, 2011, **166**, 1083–1089.
36 Q. M. Zhou, S. Wang, Z. W. Wu, Z. F. Qin, M. Dong, J. G. Wang and W. B. Fan, *Catal. Sci. Technol.*, 2023, **13**, 1009–1020.
37 N. S. de Resende, J. G. Eon and M. Schmal, *J. Catal.*, 1999, **183**, 6–13.
38 L. M. Ren, Q. M. Wu, C. G. Yang, L. F. Zhu, C. J. Li, P. L. Zhang, H. Y. Zhang, X. J. Meng and F. S. Xiao, *J. Am. Chem. Soc.*, 2012, **134**, 15173–15176.
39 Z. Y. Zakaria, J. Linnekoski and N. A. S. Amin, *Chem. Eng. J.*, 2012, **207**, 803–813.
40 M. P. Gonzalez-Marcos, E. G. Fuentes-Ordonez, J. A. Salbidegoitia and J. R. Gonzalez-Velasco, *Top. Catal.*, 2021, **64**, 224–242.
41 M. Fedyna, M. Sliwa, K. Jaroszewska and J. Trawczynski, *Fuel*, 2020, **280**, 118607.
42 H. Yan, D. L. Ren, Z. Q. Li, J. S. Chen, X. Y. Zhang, Y. H. Wang, G. Z. Duan, X. Feng, X. Zhou, Y. B. Liu, X. B. Chen and C. H. Yang, *AIChE J.*, 2022, e17974.
43 S. Y. Sang, F. X. Chang, Z. M. Liu, C. Q. He, Y. L. He and L. Xu, *Catal. Today*, 2004, **93–95**, 729–734.
44 I. N. Leontyev, S. V. Belenov, V. E. Guterman, P. Haghi-Ashtiani, A. P. Shaganov and B. Dkhil, *J. Phys. Chem. C*, 2011, **115**, 5429–5434.
45 B. Lim, M. J. Jiang, P. H. C. Camargo, E. C. Cho, J. Tao, X. M. Lu, Y. M. Zhu and Y. N. Xia, *Science*, 2009, **324**, 1302–1305.
46 W. Y. Chen, J. Ji, X. Feng, X. Z. Duan, G. Qian, P. Li, X. G. Zhou, D. Chen and W. K. Yuan, *J. Am. Chem. Soc.*, 2014, **136**, 16736–16739.
47 A. Caiola, B. Robinson, X. W. Bai, D. Shekhawat and J. L. Hu, *Ind. Eng. Chem. Res.*, 2021, **60**, 11421–11431.
48 Y. D. Wang, Z. C. Tao, B. S. Wu, J. Xu, C. F. Huo, K. Li, H. M. Chen, Y. Yang and Y. W. Li, *J. Catal.*, 2015, **322**, 1–13.
49 M. Guisnet and P. Magnoux, *Appl. Catal., A*, 2001, **212**, 83–96.
50 E. Gomez, X. W. Nie, J. H. Lee, Z. H. Xie and J. G. G. Chen, *J. Am. Chem. Soc.*, 2019, **141**, 17771–17782.

